Morphologie (2018) xxx, xxx—xxx

Disponible en ligne sur ScienceDirect www.sciencedirect.com

Elsevier Masson France EM|consulte www.em-consulte.com

ORIGINAL ARTICLE

Metaplastic woven bone in bone metastases: A Fourier-transform infrared analysis and imaging of bone quality (FTIR)

Le tissu osseux métaplasique dans les métastases osseuses : analyse et imagerie de la qualité osseuse en microscopie infra-rouge à transformée de Fourier (FTIR)

D. Chappard[a,*], G. Mabilleau[a], C. Masson[a,b], A. Tahla[c], E. Legrand[a,b]

[a] *Groupe études remodelage osseux et biomatériaux, Gerom, SFR 42—08, université d'Angers, IRIS-IBS, institut de biologie en santé, CHU d'Angers, 49933 Angers cedex, France*
[b] *Service de rhumatologie, CHU d'Angers, 49033 Angers cedex, France*
[c] *Département de chirurgie osseuse, CHU d'Angers, 49033 Angers cedex, France*

KEYWORDS
Bone metastasis;
FTIR;
Woven bone;
Osteosclerosis;
Infra-red microscopy

Summary Most osteolytic tumors are in fact mixed and contain an osteoblastic component associated with the predominant osteolytic areas. This metaplastic woven bone is always evidenced by histological analysis even in the absence of radiological expression. Metaplastic bone formation reflects the activation of new osteoblasts coming from the stimulation of the dormant lining cells. Twelve patients with secondary metastases of the iliac crest evidenced by hot spots on a ^{99}Tc-MBP san were diagnosed by histomorphometry on bone biopsies. Fourier Transformed InfraRed analysis and Imaging (FTIRI) was used on 4 μm thick sections of undecalcified bone. The mineralization degree, carbonate substitution, crystallinity and the cross-links ratio of collagen (1660/1690 cm^{-1} bands) were determined. The matrix characteristics were analyzed and imaged in the pre-existing residual bone and in the metaplastic woven bone in the vicinity of the tumor cells. FTIRI provided images of the phosphate, amide and combination of peak ratio after having selected the peaks of interest. In addition, the matrix properties can be measured and compared between the old and newly-formed bones. Woven bone appeared poorly calcified with a low phosphate/amide ratio ($P = 0.03$) crystallinity ($P < 0.0001$) and carbonate substitution ($P = 0.003$). Collagen was less mature as evidenced by lower cross-links ($P = 0.01$). Woven bone associated with bone metastasis appears poorly mineralized and rapidly elaborated

* Corresponding author.
E-mail address: daniel.chappard@univ-angers.fr (D. Chappard).

https://doi.org/10.1016/j.morpho.2018.02.002

Please cite this article in press as: Chappard D, et al. Metaplastic woven bone in bone metastases: A Fourier-transform infrared analysis and imaging of bone quality (FTIR). Morphologie (2018), https://doi.org/10.1016/j.morpho.2018.02.002

by osteoblasts. The collagenous phase of the bone matrix has a low level of reticulation. FTIRI is a powerful tool to measure and visualize the various components of the bone matrix in human diseases.

Résumé La plupart des tumeurs ostéolytiques sont en fait mixtes et contiennent un composant ostéoblastique associé aux zones ostéolytiques qui prédominent. Cet os métaplasique fibreux, non lamellaire, est toujours mis en évidence histologiquement même en l'absence d'expression radiologique. La formation d'os métaplasique reflète l'activation de nouveaux ostéoblastes provenant de la stimulation des cellules bordantes. Douze patients présentant des métastases osseuses secondaires mises en évidence par des foyers chauds en scintigraphie au ^{99}Tc-MBP ont été diagnostiqués en histomorphométrie sur des biopsies osseuses de la crête iliaque. L'analyse et l'imagerie infrarouges à transformée de Fourier (FTIRI) ont été utilisées sur des coupes de 4 μm d'épaisseur d'os non décalcifié. La minéralisation, le taux de substitution par des carbonates, la cristallinité et le rapport des cross-links du collagène (bandes à 1660/1690 cm^{-1}) ont été déterminés. Les caractéristiques de la matrice osseuse ont été analysées et imagées dans l'os résiduel préexistant et dans l'os métaplasique au voisinage des cellules tumorales. La FTIRI a fourni des images de la distribution des phosphates, des amides et des rapports de combinaisons de pics après avoir sélectionné les pics d'intérêt. De plus, les propriétés de la matrice ont pu être mesurées et comparées entre l'os résiduel et l'os métaplasique. Ce dernier est apparu faiblement calcifié avec un rapport phosphate/amide ($p = 0,03$), une cristallinité ($p < 0,0001$) et une substitution carbonate ($p = 0,003$) réduits. Le collagène était moins mature comme en témoignent une plus faible quantité de cross-links ($p = 0,01$). L'os métaplasique au cours des métastases osseuses apparaît faiblement minéralisé et rapidement élaboré par les ostéoblastes. La phase collagénique de la matrice osseuse présente un faible taux de réticulation. La FTIRI est un outil puissant pour mesurer et visualiser les différents composants de la matrice osseuse dans les ostéopathies humaines.

Introduction

In patients with advanced cancer, bone is frequently involved, particularly is the case of breast and prostate adenocarcinomas that have been recognized as highly osteophilic tumors several centuries ago [1,2]. In these two types of malignancies, bone metastases are observed in 60—70% of patients. Malignant cells have a particular propensity for homing to the bone morrow since they express various chemokines or synthetize various proteins that favor their anchorage in the bone marrow microenvironment. Bone marrow, in turn, can provide a ''fertile soil'' for the growth of metastatic cells: a large number of growth factors and cytokines are naturally present to control the growth and differentiation of hematopoietic cells [3]. Also, bone remodeling (which is normally maintained at equilibrium by a complex network of cytokines) is altered by malignant cells. After arrival in the bone marrow microenvironment, tumor cells interact with bone remodeling and disrupt the coordinated action of osteoclasts (bone resorbing cells) and osteoblasts (bone forming cells) [4]. Typically metastases are usually considered as osteosclerotic or osteolytic, based on the X-ray appearance of the bone lesions [5]. Osteoclerotic metastases are common in prostate cancer while lung, breast, kidney or gut tumors typically produce osteolytic metastases. However, most of the osteolytic tumors are in fact mixed and contain an osteoblastic component associated with the predominant osteolytic areas. This osteoblastic component is stimulated by the release of growth factors (secreted by the malignant cells such as endothelin-1) or buried in the bone matrix during the osteoclastic resorption phase [6,7]. Among them, transforming growth factor β (TGF-β) is stored at high concentrations. Several studies have reported that it can activate tumor cell progression via the *smad* pathway, this producing a ''vicious circle'' between malignant and bone cells [8]. During the physiological remodeling process, TGF-β controls the coupling between bone formation and resorption. TGF-β inhibits osteoclast differentiation and promotes the recruitment of new osteoblasts in the eroded areas. In osteolytic metastases, osteoclast activity is considerably increased (by a number of cytokines released by the tumor cells), thus releasing high amount of TGF-β that can provoke the formation of metaplastic bone in the vicinity of the osteolytic foci [8,9].

Recently, new histological methods have appeared to characterize the quality of the bone matrix in human diseases. Fourier transformed infrared analysis and imaging (FTIRI) is an interesting technique for imaging the mineral and the organic phases of the matrix in tissue sections [10,11]. The aim of the present retrospective study was to analyze the bone matrix in patients with mixed metastases containing a noticeable amount of woven bone. Undecalcified bone sections were used and the matrix characteristics

Please cite this article in press as: Chappard D, et al. Metaplastic woven bone in bone metastases: A Fourier-transform infrared analysis and imaging of bone quality (FTIR). Morphologie (2018), https://doi.org/10.1016/j.morpho.2018.02.002

Table 1 Patients characteristics with type of metastasis on X-ray images and osteoid parameters determined by histomorphometry.

Patient	Gender	X-ray	Tumor origin	OV/BV (%)	OS/BS (%)	O.Th (μm)
1	Female	Mixed	Breast	8.8[a]	45.7[a]	11.9
2	Male	Osteosclerosis	Lung	12.6[a]	75.6[a]	21.9[a]
3	Male	Mixed	Prostate	2.5	13.3	13.6
4	Male	Osteosclerosis	Prostate	22.7[a]	100[a]	27.9[a]
5	Male	Osteosclerosis	Prostate	2.9	13.9	10.9
6	Male	Osteosclerosis	Prostate	12.9[a]	32.6[a]	14.1
7	Male	Osteosclerosis	Prostate	31.6[a]	59.1[a]	24.3[a]
8	Female	Mixed	Unknown	2.9	11.2	14.3
9	Male	Osteosclerosis	Unknown	29.0[a]	100[a]	27.3[a]
10	Female	Mixed	Breast	6.2[a]	12.1	14.8[a]
11	Female	Mixed	Breast	7.8[a]	25.5[a]	9.5
12	Female	Osteosclerosis	Breast	17.9[a]	69.1[a]	15.7[a]

[a] Increased vs. normal values, i.e. < 6% for osteoid volume OV/BV; < 20% for osteoid surfaces OS/BS and 15 μm for osteoid thickness O.Th.

were determined and imaged in the pre-existing residual bone and in the newly-formed bone in the vicinity of the tumor cells.

Patients

Twelve patients (five females, seven males) from the rheumatology unit were referred for the histopathological diagnosis of a bone metastasis at the ilium. The characteristics of patients are given in Table 1. All patients had a ^{99}Tc—MBP bone scan that evidenced hot lesions. Seven patients presented osteosclerotic lesions and five had mixed bony lesions associating sclerotic and lytic foci on X-rays. Transiliac bone biopsy was done in these areas under local anesthesia as previously reported [12]. Six patients had a single tetracycline bone labeling done with demethylchlortetracyline (150 mg/d during two days) to evaluate the extent of osteoid surfaces with active mineralization. The Ethical Subcommittee of our university hospital approved the use of patient material as this work is retrospective from a bone sample collection (complementary histological study).

Material and methods

Bone biopsies

A transiliac bone biopsy was obtained in all patients under local anesthesia with a 7 mm internal diameter trephine, 2 cm below the iliac crest and 2 cm behind the antero-superior iliac spine (Commeca, 49070 Beaucouzé, France). Specimens were fixed in an ethanol-based fluid [13]. Bone cores were fixed for 24 hours, dehydrated in acetone and embedded undecalcified in poly (methylmethacrylate) (pMMA) Sections (7 μm in thickness for histomorphometry and 4 μm for FTIRI) were cut dry on a heavy duty microtome equipped with tungsten carbide knives (Leica Polycut S with 50 knives). They were stained with Goldner's trichrome for the identification of osteoid and hematoxylin-phloxin-saffron (HPS) for cytological examination. Osteoclasts were detected by an histoenzymologic method based on the tartrate resistant acid phosphatase (TRAcP) determination [14]. A complete histomorphometric analysis was done according to the recommendations of the American Society for Bone and Mineral Research [15]. Only osteoid parameters (osteoid volume, surface and thickness) were considered here.

Fourier-transform infrared microspectroscopy (FTIR and FTIRI)

Analysis was done according to previous specifications on 4 μm thick sections [16,17]. Sections were sandwiched between two barium fluoride (BaF2) optical windows (IR grade). Samples were then analyzed with a Bruker Hyperion 3000 microscope (Bruker optic, Ettlingen, Germany) equipped with a liquid nitrogen-cooled Mercury Cadmium Telluride (MCT) detector and purged with dried air, and interfaced with a vertex 70 spectrometer (Bruker). A 15X Cassegrain objective and condenser with a numerical aperture of 0.4 were used. Infrared spectra were collected at a spectral resolution of 4 cm^{-1} in transmission mode on 32 co-added scans. FTIR data processing was performed with the Bruker's proprietary Opus Software (release 6.5). A background spectrum was collected, containing data from the environment, the instrument and the optical disks. Sequential raw spectra for each regions analyzed were averaged and the contribution of the embedding pMMA was spectrally subtracted after normalization of the peak located at 1730 cm^{-1}. Twenty spectra (15 μm apart in a 45 × 60 μm square matrix) were obtained in three different regions of independent trabeculae per bone samples. Analysis was done separately in the pre-existing and in thin trabeculae composed of metaplastic woven bone. In all instances, at least five trabeculae were analyzed from each section in the two different locations. Spectra were cut between 800—1800 cm^{-1}, baseline corrected with an elastic correction method, vector normalized in the amide 1 region (1585—1710 cm^{-1}) and averaged. Spectra were also subjected to curve fitting in the $\upsilon 1$ $\upsilon 3$ phosphate

Please cite this article in press as: Chappard D, et al. Metaplastic woven bone in bone metastases: A Fourier-transform infrared analysis and imaging of bone quality (FTIR). Morphologie (2018), https://doi.org/10.1016/j.morpho.2018.02.002

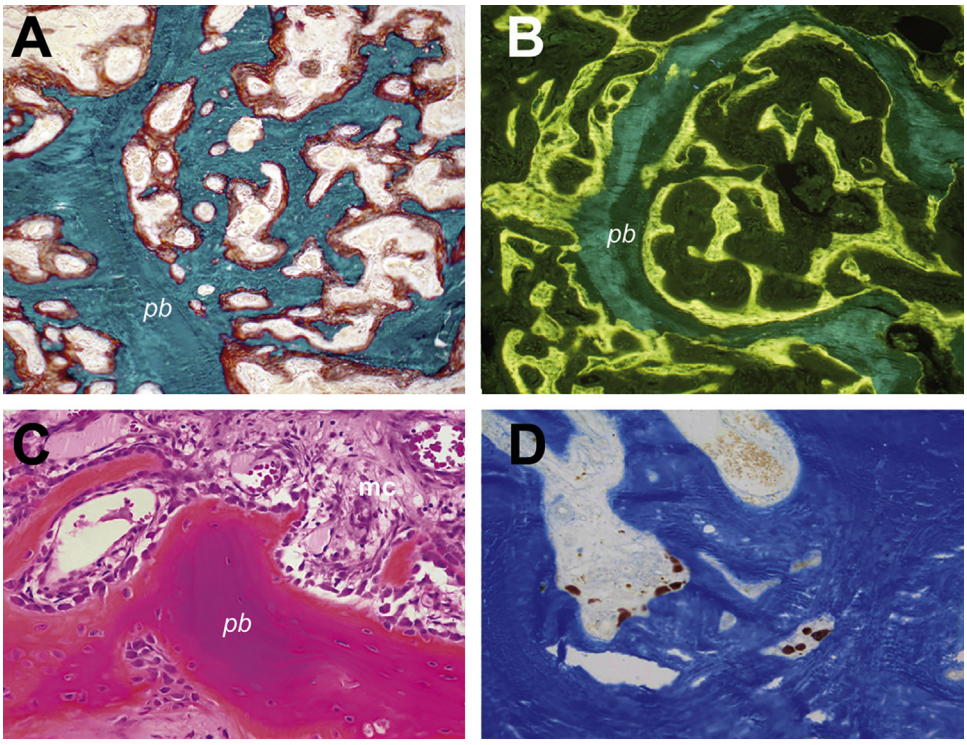

Figure 1 Histological findings in biopsies from patients with bone metastasis associated with woven bone. A. Prostate adenocarcinoma: note the considerable extent of thin neo-trabeculae made of woven bone and covered with osteoid tissue (in red) and anchored at the surface of pre-existing trabeculae (pb); Goldner's trichrome. B. Same patient, undecalcified bone section showing the considerable extent of fixation of tetracycline in actively mineralizing surfaces. C. Patient with a breast adenocarcinoma. Note the considerable stimulation of osteoblastogenesis and the appearance of new bone (orange) laid on pre-existing bone (pb); Mc: malignant cells and stroma reaction. D. Histoenzymological identification of numerous osteoclasts (in brown) by the TRAcP reaction in a patient with a sclerosis metastasis from a prostate adenocarcinoma.

band (900—1200 cm^{-1}) and the amide I- amide II region (1485—1720 cm^{-1}) according to second derivative and the Levenberg-Maquardt algorithm using the Grams/AI 8.0 software as reported previously [18].

The evaluated IR spectral parameters were:

- mineral to matrix ratio, calculated as the integrated area of the $\nu 1$ $\nu 3$ phosphate band over the amide 1 region (1585—1720 cm^{-1}) and used as an index of mineral content [10];
- mineral crystallinity, which reflects the apatite size and perfection and calculated as the area ratio of the 1020 cm^{-1} over the 1030 cm^{-1} subbands [11]. A lower ratio indicates a higher mineral crystallinity;
- collagen maturity, related to the relative proportion of the two major collagen cross-links pyridinium (Pyr, non-reducible) and deH-DHLNL (reducible) and calculated as the area ratio of the 1660 and 1690 cm^{-1} subbands [19];
- carbonates to phosphates ratio, which reflects the carbonate content in bone and calculated as ratio of integrated areas of the $\upsilon 2$ CO_3^{2-} region (850—890 cm^{-1}) and $\nu 1$ $\nu 3$ phosphate band [20].

For FTIRI, sections were imaged using a 64×64 element focal plane array (FPA) detector (coupled with the microscope) to provide 4096 spectra simultaneously from interest areas. The images were collected at a resolution of 8 cm^{-1} with 32 co-added scans for background and samples, in the transmission mode in the spectral region 900—2000 cm^{-1}. Images of the trabeculae were obtained by a stitching of 3×3 elemental images provided by the FPA with the Opus software. Three spectral images were acquired on separated area from each sample, each area containing an pre-existing trabecular and foci of woven bone. Each image was ratioed against the background imaging spectra collected under identical conditions. Color-coded images of mineral to matrix ratio, mineral cristallinity, collagen maturity and carbonate content (using the intensity of the $\nu 3$ carbonate band at 1415 cm^{-1} over the $\nu 1 \nu 3$ phosphate band distributions were produced in each groups for qualitative comparison by using a Matlab routine (release 7.10; Math Works, Natick, MA) [21]. The spectroscopic calculated parameters were expressed as a color-coded images, the color of a pixel corresponding to a certain range of values.

Statistical analysis

Statistical analysis was performed with the Systat® statistical software release 11.0 (Systat inc. San José; CA). Data are expressed as mean $\pm$ SD. Differences between groups were analysed by the non-parametric Mann and Whitney *U* test. Differences were considered significant when $P < 0.05$.

Please cite this article in press as: Chappard D, et al. Metaplastic woven bone in bone metastases: A Fourier-transform infrared analysis and imaging of bone quality (FTIR). Morphologie (2018), https://doi.org/10.1016/j.morpho.2018.02.002

Results

Histological analysis

In this series of patients, the origin of the primary tumor was a breast adenocarcinoma in four cases, five prostate adenocarcinoma, one lung adenocarcinoma and two cases with adenocarcinomas from an unknown origin. In all cases, the histological examination revealed numerous foci of metaplastic bone (woven bone) anchored at the surface of the previous trabeculae from the patient (''old bone'') inside the cancellous space (Fig. 1A). In the patient with the lung adenocarcinoma, metaplastic bone was also observed under the periosteum. The woven texture could easily be observed under polarization microscopy. The osteoid parameters were increased in nine patients indicating an increased osteoblastic activity (Table 1) and the amount of metaplastic bone differed between the patients and those with prostate adenocarcinoma had the highest amount of metaplastic bone that tended to completely fill the marrow cavity. These thin trabeculae appeared with a green core when stained by Goldner's trichrome and were covered by thick osteoid seams. O.Th was increased in six patients indicating an altered mineralization. In patients with tetracycline labeling, the metaplastic bone was heavily labeled by the fluorescent marker (Fig. 1B). On HPS stained sections, the metastatic cells supported by the collagenous stroma

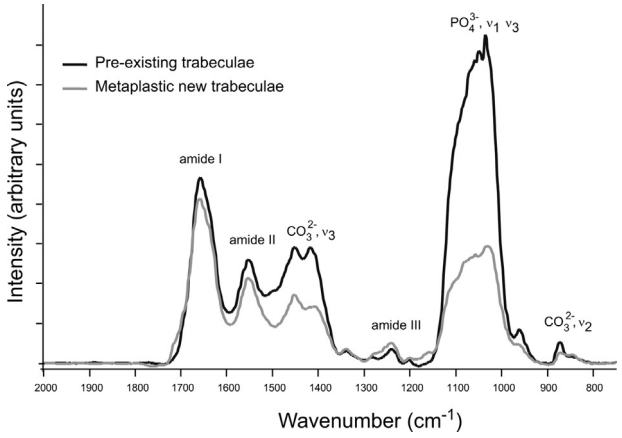

Figure 2 Typical FTIR spectrum of the bone matrix in a patient with metastasis comprising woven bone anchored at the surface of pre-existing bone. Pre-existing trabeculae: black spectrum; woven bone from the metaplastic new trabeculae: grey curve.

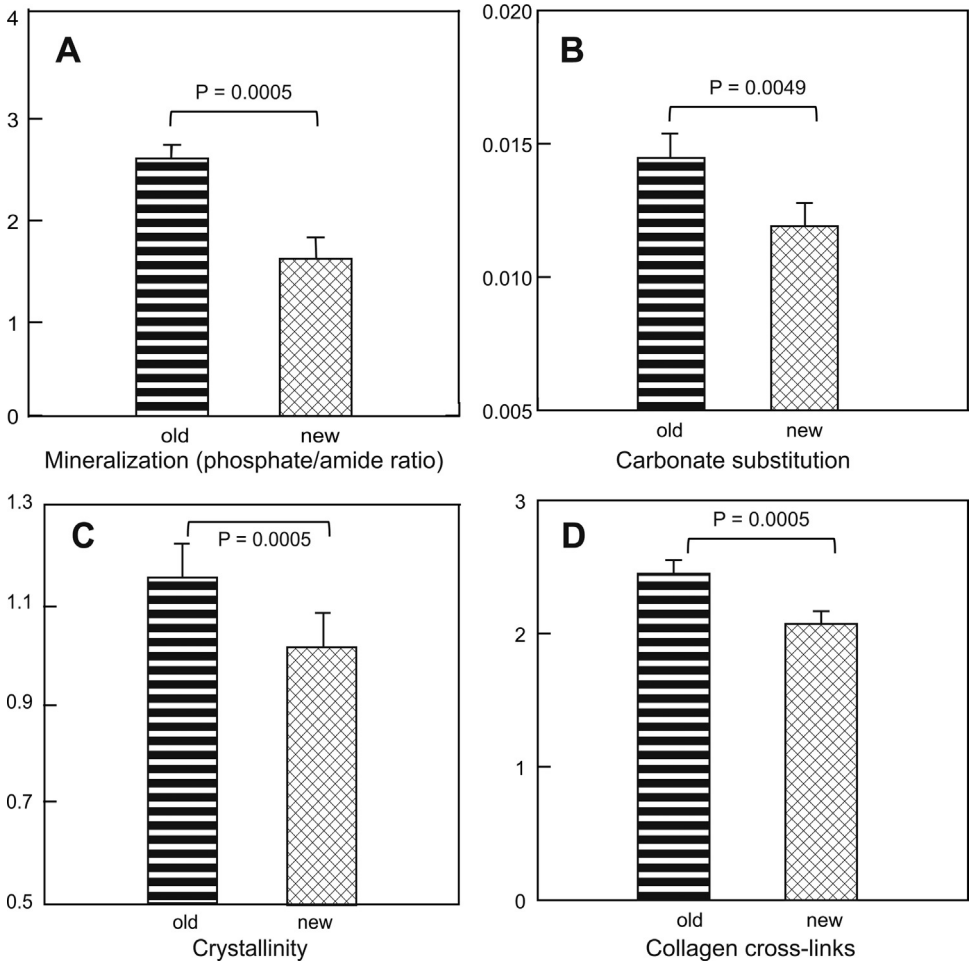

Figure 3 Parameters derived from FTIR spectra measured in the pre-existing bone and the newly-formed trabeculae in patients with bone metastases. A. Mineral to organic matric ratio. B. Carbonate substitution. C. Crystallinity. D. Collagen cross-links. Abscissa axes: arbitrary units.

Please cite this article in press as: Chappard D, et al. Metaplastic woven bone in bone metastases: A Fourier-transform infrared analysis and imaging of bone quality (FTIR). Morphologie (2018), https://doi.org/10.1016/j.morpho.2018.02.002

reaction could be evidenced. Numerous pseudo-epithelial seams of osteoblasts, apposing new bone at the surface of the pre-existing trabeculae, were also evidenced (Fig. 1C). TRAcP stained sections evidenced numerous foci of active osteoclasts in eroded areas dug in the vicinity of the malignant cells (Fig. 1D). Osteoclasts were found at the surface of pre-existing trabeculae but they also appeared to remodel the metaplastic bone.

FTIR analysis

The typical spectrum of the bone matrix was different in the pre-existing bone and in the metaplastic bone from the newly-formed trabeculae (Fig. 2). The $\nu 1$ $\nu 2$ phosphate peak was markedly reduced in the metaplastic trabeculae. The indexes from the FTIR spectra appear on Fig. 3. Mineralization (phosphate/amide I ratio) was significantly reduced in new bone when compared to the pre-existing bone from pre-existing trabeculae. Similarly, the carbonate substitution, crystallinity and the amount of cross-links were reduced in the woven bone from the metaplastic foci.

FTIRI analysis

FTIRI analysis confirmed these results and provided 2D spatial imaging of the molecular maps derived from the FTIR spectra. Examples of typical images are given for a metastasis from a breast cancer (Fig. 4) and from a prostate cancer (Fig. 5). The amount of phosphate was markedly reduced in the thin metaplastic trabeculae (Figs. 4B—5B) and the surface area of the woven bone was less than noted on the video images (Figs. 4A—5A). On the contrary, the amide I map identified a larger area because collagen was also present in the osteoid seams that cover all these trabeculae and anchor them on the pre-existing ones (Figs. 4C—5C). The map of the cross-links confirmed that they were by far less numerous in these newly-formed metaplastic trabeculae than in the pre-existing trabecular bone (Figs. 4D—5D).

Discussion

In this series of patients with metastatic adenocarcinomas at the iliac bone, foci of woven bone were always identified at the surface of the pre-existing trabeculae in the cancellous space; they have a typical candelabra aspect with thin trabeculae. In the patient with a lung cancer, the presence of woven bone also extending in the sub-periosteal areas is also characteristic of a marrow metastasis [22]. All patients had a bone metastasis that was clinically classified either as osteosclerotic or mixed on X-rays. In addition, only patients with hot spots on the ^{99}Tc-MBP bone scan were selected prior

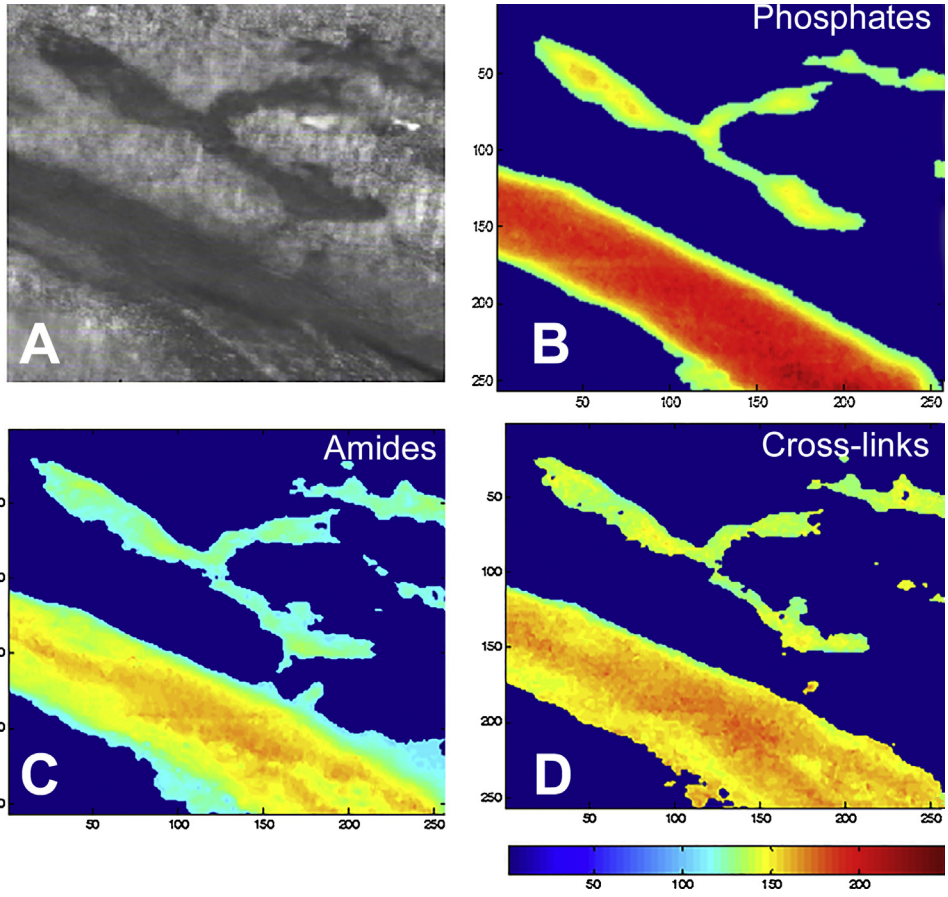

Figure 4 FTIRI images obtained in a female patient with metastasis from a breast adenocarcinoma. A. Video image of a 4 μm thick undecalcified section. B. Spatial distribution of phosphates. C. Spatial distribution of the amide groups of collagen. D. Spatial distribution of the collagen cross-links, note the reduce content in the woven bone. The look-up table is given at the bottom.

Please cite this article in press as: Chappard D, et al. Metaplastic woven bone in bone metastases: A Fourier-transform infrared analysis and imaging of bone quality (FTIR). Morphologie (2018), https://doi.org/10.1016/j.morpho.2018.02.002

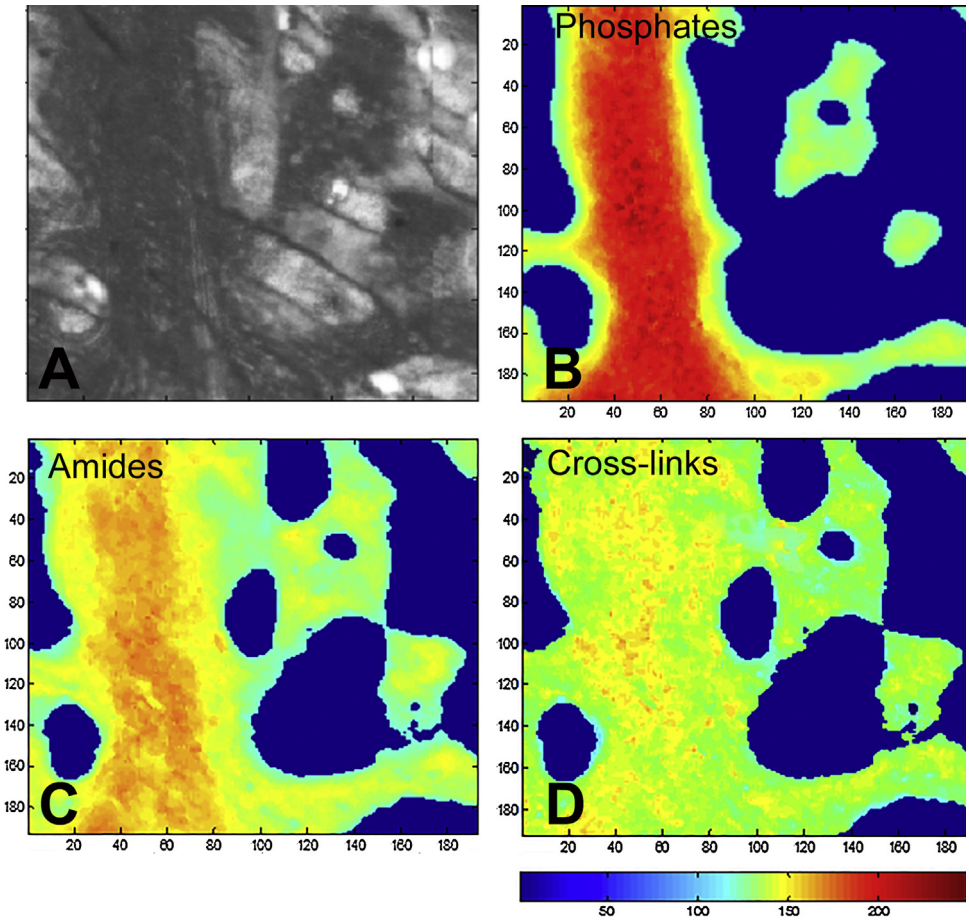

Figure 5 FTIRI images obtained in a male patient with sclerosis metastasis from a prostate adenocarcinoma. A. Video image of a 4 μm thick undecalcified section. B. Spatial distribution of phosphates, the pre-existing bone has a higher phosphate content. C. Spatial distribution of the amide groups of collagen of both the mineralized woven bone and osteoid tissue. D. Spatial distribution of the collagen cross-links, note the reduce content in the woven bone. The look-up table is given at the bottom.

to analysis because it indicates a high osteoblastic activity causing an elevated uptake of the radionuclide-labeled bisphosphonate [23]. Some types of cancers such as breast and prostate adenocarcinomas are specially metastasizing to bone, because they possess unique capacities that facilitate their anchoring in the marrow [2,5].

Osteoblastic activity is increased in metaplastic trabeculae with plumped cells and enlarged osteocytes [24]. This metaplastic bone may be evidenced as buried white areas on X-rays but is always evidenced by histology even in the absence of radiological expression [25]. Metaplastic bone formation reflects the activation of new osteoblasts or the stimulation of the dormant lining cells at the surface of bone trabeculae. They elaborate rapidly plexiform trabeculae made of woven bone, which are anchored on the pre-existing bone surfaces as shown by histology or microcomputed tomography [7,26—28]. The bone matrix is made of randomly disposed bundles of collagen fibers which are secondarily mineralized. Metaplastic bone is formed by either the release of growth factors by the tumor (e.g., endothelin-1 and IL-6 in prostate carcinoma) or due to the excess in osteoclastic activity which release locally high amounts of TGF-β which is buried in the bone matrix [29,30].

In this study, we found that the bone matrix of the newly-formed bone trabeculae was incompletely mineralized with a marked decrease in mineral crystallinity (i.e. poorly made hydroxyapatite crystals). A reduction in the carbonate/phosphate ratio also indicates an immature bone matrix since the β-carbonate substitution (i.e., replacement of a phosphate group by a carbonate in the hydroxyapatite crystal) increases upon aging [31,32]. Similar finding were observed in rats which developed sclerosing metastases after injection of LNCaP C4-2B prostate cancer cells in the tibia. Raman microspectroscopy identifies a decrease in the mineralization degree and hydroxyapatite crystallinity [33].

Woven bone is synthetized by osteoblasts with an anarchic texture in which collagen fibers have random directions. This bone also mineralizes rapidly and is reported to have an higher degree of mineralization than lamellar bone [34]. However, its biomechanical properties are poorer than those of lamellar bone because the irregular collagen-fibril orientation and higher mineralization degree make it capable to absorb less energy [35,36]. It should however be noted that these studies were conducted in the growing skeleton of healthy animals. In this study, woven bone was observed in a pathologic condition where the neoplastic cells have

Please cite this article in press as: Chappard D, et al. Metaplastic woven bone in bone metastases: A Fourier-transform infrared analysis and imaging of bone quality (FTIR). Morphologie (2018), https://doi.org/10.1016/j.morpho.2018.02.002

considerably increased the activity of osteoblasts. The consequence is that the newly-formed bone is incompletely mineralized with a reduced collagen maturity in the bone matrix. Similar findings have been observed around dental implants: the placement of a dental implant is followed by rapid deposition of woven bone allowing a primary anchorage but the degree of mineralization and biomechanical properties are reduced when compared with lamellar bone [37,38]. In fibrous bone dysplasia, the lamellar texture of bone is replaced by woven bone, which is less mineralized and has a reduced mechanical strength [39,40]. In bone metastases, the presence of a high amount of incompletely calcified bone has sometimes important consequences on calcium metabolism: hypocalcemia is a metabolic disturbance which is common in advanced prostate or breast cancer due to the ''hungry bone'' syndrome [41,42]. In such patients, the increase in the amount of woven bone and osteoblastic activity are responsible for an increase trapping of calcium in the sclerosis areas. Treatment with bisphosphonates is the standard of care for patients with breast cancer who have predominantly osteolytic lesions as these compounds have a marked anti-osteoclastic activy. However, bisphosphonates are now known to depress both osteoclastic and osteoblastic activity in a second time due to the coupling between these cell populations during the remodeling process. Bisphosphonates are now used to reduce the bone forming activity thus avoiding the ''hungry bone syndrome'' [43,44].

Conclusion

Metaplastic bone present in bone metastases from different types of adenocarcinoma are built by stimulated osteoblasts from the tumor. They rapidly elaborate trabeculae made of woven bone anchored at the surface of the pre-existing trabeculae but woven bone has a poor quality. The mineral to matrix ratio was markedly reduced (evidencing a low mineralization degree), the carbonate content and crystallinity were reduced (indicating a poor maturation of hydroxyapatite), and the collagen maturity was reduced with a low amount of cross-links. The amount of this woven bone with a poor quality may have clinical consequences.

Disclosure of interest

The authors declare that they have no competing interest.

Acknowledgements

Authors thank Mrs. Laurence Lechat for secretarial assistance. They also thank Mrs Christine Audrain and Aleksandra Mieczkowska for her skillful technical assistances with FTIRI. This work was supported by financial participation of the French Ministry for Research.

References

[1] Coleman RE. Skeletal complications of malignancy. Cancer 1997;80:1588—94.
[2] Guise TA, Mundy GR. Cancer and bone. Endocr Rev 1998;19:18—54.
[3] Fidler IJ. The pathogenesis of cancer metastasis: the ''seed and soil'' hypothesis revisited. Nat Rev Cancer 2003;3:453—8.
[4] Rizzoli R, Body JJ, Brandi ML, Cannata-Andia J, Chappard D, El Maghraoui A, et al. Cancer-associated bone disease. Osteoporos Int 2013;24:2929—53.
[5] Clézardin P, Teti A. Bone metastasis: pathogenesis and therapeutic implications. Clin Exp Metastasis 2007;24:599—608.
[6] Fournier PGJ, Juárez P, Guise TA. Tumor-bone interactions: there is no place like bone. In: Heymann D, editor. Bone cancer: progression and therapeutic approaches. 2nd Ed. London: Acad. Press; Elsevier Inc.; 2014. p. 13—28.
[7] Chappard D, Bouvard B, Baslé MF, Legrand E, Audran M. Bone metastasis: histological changes and pathophysiological mechanisms in osteolytic or osteosclerotic localizations. A review. Morphologie 2011;95:65—75.
[8] Baselga J, Rothenberg ML, Tabernero J, Seoane J, Daly T, Cleverly A, et al. TGF-beta signalling-related markers in cancer patients with bone metastasis. Biomarkers 2008;13:217—36.
[9] Guise TA, Chirgwin JM. Transforming growth factor-beta in osteolytic breast cancer bone metastases. Clin Orthop Relat Res 2003;415S:32—8.
[10] Boskey AL, Pleshko N, S.B. D, Mendelsohn R. Applications of Fourier transform infrared (FT-IR) microscopy to the study of mineralization in bone and cartilage. Cells Mater 1992;2:209—20.
[11] Paschalis EP, DiCarlo E, Betts F, Sherman P, Mendelsohn R, Boskey AL. FTIR microspectroscopic analysis of human osteonal bone. Calcif Tissue Int 1996;59:480—7.
[12] Audran M, Maury E, Bouvard B, Legrand E, Baslé MF, Chappard D. Is transiliac bone biopsy a painful procedure? Clin Nephrol 2012;77:97—104.
[13] Beebe K. Alcohol/xylene: the unlikely fixative/dehydrant/clearant. J Histotechnol 2000;23:45—50.
[14] Chappard D. Technical aspects: how do we best prepare bone samples for proper histological analysis? In: Heymann D, editor. Bone cancer: progression and therapeutic approaches. 2nd Ed. London: Acad. Press; Elsevier Inc.; 2014. p. 111—20.
[15] Dempster DW, Compston JE, Drezner MK, Kanis JA, Malluche H. Standardized nomenclature, symbols, and units for bone histomorphometry: a 2012 update of the report of the ASBMR Histomorphometry Nomenclature Committee. J Bone Miner Res 2013;28:2—17.
[16] Gamsjaeger S, Mendelsohn R, Boskey AL, Gourion-Arsiquaud S, Klaushofer K, Paschalis EP. Vibrational spectroscopic imaging for the evaluation of matrix and mineral chemistry. Curr Osteoporos Rep 2014;12:454—64.
[17] Paschalis EP. Fourier transform infrared imaging of bone. Methods Mol Med 2012;816:517—25.
[18] Mieczkowska A, Bouvard B, Chappard D, Mabilleau G. Glucose-dependent insulinotropic polypeptide (GIP) directly affects collagen fibril diameter and collagen cross-linking in osteoblast cultures. Bone 2015;74C:29—36.
[19] Paschalis EP, Verdelis K, Doty SB, Boskey AL, Mendelsohn R, Yamauchi M. Spectroscopic characterization of collagen cross-links in bone. J Bone Miner Res 2001;16:1821—8.
[20] Boskey AL, DiCarlo E, Paschalis E, West P, Mendelsohn R. Comparison of mineral quality and quantity in iliac crest biopsies from high- and low-turnover osteoporosis: an FT-IR microspectroscopic investigation. Osteoporos Int 2005;16:2031—8.
[21] Ou-Yang H, Paschalis EP, Mayo WE, Boskey AL, Mendelsohn R. Infrared microscopic imaging of bone: spatial distribution of CO_3(2-). J Bone Miner Res 2001;16:893—900.
[22] Wlodarski KH, Reddi HA. Tumor cells stimulate in vivo periosteal bone formation. Bone Miner 1987;2:185—92.
[23] Nome R, Hernes E, Bogsrud TV, Bjøro T, Fosså SD. Changes in prostate-specific antigen, markers of bone metabolism and

bone scans after treatment with radium-223. Scand J Urol 2015;49:211—7.
[24] Chappard D, Laurent JL, Bousquet G, Riffat G, Odelin MF. Mean osteoplastic surface in zones of plexiform neo-osteogenesis compared with mean osteoplastic surface measured on the fetal bone. Bull Assoc Anat 1978;62:389—99.
[25] Vukmirovic-Popovic S, Escott NG, Duivenvoorden WC. Presence and enzymatic activity of prostate-specific antigen in archival prostate cancer samples. Oncol Rep 2008;20:897—903.
[26] Chappard D, Libouban H, Legrand E, Ifrah N, Masson C, Baslé MF, et al. Computed microtomography of bone specimens for rapid analysis of bone changes associated with malignancy. Anat Rec 2010;293:1125—33.
[27] Schmidt A, Blanchet O, Dib M, Baslé MF, Ifrah N, Chappard D. Bone changes in myelofibrosis with myeloid metaplasia: a histomorphometric and microcomputed tomographic study. Eur J Haematol 2007;78:500—9.
[28] Chappard D. Bone and cancer (metastasis and hematologic disorders [Tissu osseux et pathologies cancéreuses (métastases et maladies hématologiques)]. In: Guillaume B, Audran M, Chappard D, editors. Tissu osseux et biomatériaux en chirurgie dentaire. Paris: Quintessence International; 2014. p. 209—32.
[29] Yavropoulou MP, Yovos JG. The role of the Wnt signaling pathway in osteoblast commitment and differentiation. Hormones 2007;6:279—94.
[30] Chiechi A, Waning DL, Stayrook KR, Buijs JT, Guise TA, Mohammad KS. Role of TGF-β in breast cancer bone metastases. Adv Biosci Biotechnol 2013;4:15—30.
[31] Akkus O, Adar F, Schaffler MB. Age-related changes in physicochemical properties of mineral crystals are related to impaired mechanical function of cortical bone. Bone 2004;34:443—53.
[32] Paschalis EP, Mendelsohn R, Boskey AL. Infrared assessment of bone quality: a review. Clin Orthop Rel Res 2011;469:2170—8.
[33] Bi X, Sterling JA, Merkel AR, Perrien DS, Nyman JS, Mahadevan-Jansen A. Prostate cancer metastases alter bone mineral and matrix composition independent of effects on bone architecture in mice—A quantitative study using micro CT and Raman spectroscopy. Bone 2013;56:454—60.
[34] Currey J. Mechanical properties of vertebrate hard tissues. Proc Institut Mechanic Engin Part H. J Engin Med 1998;212:399—411.
[35] Gorski JP. Is all bone the same? Distinctive distributions and properties of non-collagenous matrix proteins in lamellar vs. woven bone imply the existence of different underlying osteogenic mechanisms. Crit Rev Oral Biol Med 1998;9:201—23.
[36] Mulder L, Koolstra JH, den Toonder JM, van Eijden TM. Relationship between tissue stiffness and degree of mineralization of developing trabecular bone. J Biomed Mater Res — Part A 2008;84:508—15.
[37] Brunski JB. In vivo bone response to biomechanical loading at the bone/dental-implant interface. Adv Dent Res 1999;13:99—119.
[38] Grizon F, Aguado E, Huré G, Baslé MF, Chappard D. Enhanced bone integration of implants with increased surface roughness: a long term study in the sheep. J Dent 2002;30:195—203.
[39] Chapurlat RD, Orcel P. Fibrous dysplasia of bone and McCune — Albright syndrome. Best Pract Res Clin Rheumatol 2008;22:55—69.
[40] DiCaprio MR, Enneking WF. Fibrous dysplasia: pathophysiology, evaluation, and treatment. J Bone Joint Surg Am 2005;87:1848—64.
[41] Berruti A, Dogliotti L, Bitossi R, Fasolis G, Gorzegno G, Bellina M, et al. Incidence of skeletal complications in patients with bone metastatic prostate cancer and hormone refractory disease: predictive role of bone resorption and formation markers evaluated at baseline. J Urol 2000;164:1248—53.
[42] Carroll R, Matfin G. Endocrine and metabolic emergencies: hypocalcaemia. Ther Adv Endocrinol Metab 2010;1:29—33.
[43] Rosen L, Harland SJ, Oosterlinck W. Broad clinical activity of zoledronic acid in osteolytic to osteoblastic bone lesions in patients with a broad range of solid tumors. Am J Clin Oncol 2002;25:S19—24.
[44] Saad F. Zoledronic acid significantly reduces pathologic fractures in patients with advanced-stage prostate cancer metastatic to bone. Clin Prostate Canc 2002;1:145—52.

Please cite this article in press as: Chappard D, et al. Metaplastic woven bone in bone metastases: A Fourier-transform infrared analysis and imaging of bone quality (FTIR). Morphologie (2018), https://doi.org/10.1016/j.morpho.2018.02.002